THE JOURNAL OF PHYSICAL CHEMISTRY B

ARTICLE

pubs.acs.org/JPCB

Molecular Conformations in the Pentasaccharide LNF-1 Derived from NMR Spectroscopy and Molecular Dynamics Simulations

Elin Säwén,[†] Baltzar Stevensson,[‡] Jennie Östervall,[†,‡] Arnold Maliniak,[‡] and Göran Widmalm*[,†]

[†]Department of Organic Chemistry and [‡]Division of Physical Chemistry, Arrhenius Laboratory, Stockholm University, S-106 91 Stockholm, Sweden

ABSTRACT: The conformational dynamics of the human milk oligosaccharide lacto-*N*-fucopentaose (LNF-1), α-L-Fuc*p*-(1 → 2)-β-D-Gal*p*-(1 → 3)-β-D-Glc*p*NAc-(1 → 3)-β-D-Gal*p*-(1 → 4)-D-Glc*p*, has been analyzed using NMR spectroscopy and molecular dynamics (MD) computer simulations. Employing the Hadamard ^{13}C-excitation technique and the J-HMBC experiment, ^{1}H,^{13}C trans-glycosidic *J* coupling constants were obtained, and from one- and two-dimensional ^{1}H,^{1}H T-ROESY experiments, proton−proton cross-relaxation rates were determined in isotropic D_2O solution. In the lyotropic liquid-crystalline medium consisting of ditetradecylphosphatidylcholine, dihexylphosphatidylcholine, *N*-cetyl-*N*,*N*,*N*-trimethylammonium bromide, and D_2O, ^{1}H, ^{1}H and one-bond ^{1}H, ^{13}C residual dipolar couplings (RDCs), as well as relative sign information on homonuclear RDCs, were determined for the pentasaccharide. Molecular dynamics simulations with explicit water were carried out from which the internal isomerization relaxation time constant, τ_N, was calculated for transitions at the ψ torsion angle of the β-(1 → 3) linkage to the lactosyl group in LNF-1. Compared to the global reorientation time, τ_M, of ∼0.6 ns determined experimentally in D_2O solution, the time constant for the isomerization relaxation process, $\tau_{N(\mathrm{scaled})}$, is about one-third as large. The NMR parameters derived from the isotropic solution show very good agreement with those calculated from the MD simulations. The only notable difference occurs at the reducing end, which should be more flexible than observed by the molecular simulation, a conclusion in complete agreement with previous ^{13}C NMR relaxation data. A hydrogen-bond analysis of the MD simulation revealed that inter-residue hydrogen bonds on the order of ∼30% were present across the glycosidic linkages to sugar ring oxygens. This finding highlights that intramolecular hydrogen bonds might be important in preserving well-defined structures in otherwise flexible molecules. An analysis including generalized order parameters obtained from nuclear spin relaxation experiments was performed and successfully shown to limit the conformational space accessible to the molecule when the number of experimental data are too scarce for a complete conformational analysis.

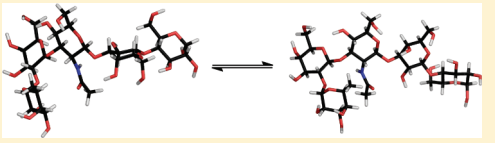

INTRODUCTION

NMR spectroscopy has a unique position in studies of biomolecules in that structure and dynamics can be investigated at atomic resolution. Furthermore, interactions between molecules can also be investigated with different NMR techniques.[1] Several NMR observables such as chemical shifts, spin−spin coupling constants, and nuclear spin relaxation times are very useful in describing the structure and dynamics of biomolecules such as proteins, nucleic acids, and carbohydrates.[2−4]

The latter class of molecules poses particular problems because of the narrow spectral range of the corresponding NMR signals. Notably, for analysis of their three-dimensional structure, in most cases, only a single strong nuclear Overhauser effect is observed across each glycosidic linkage of an oligosaccharide. A complementary way to describe the conformational preference(s) at a glycosidic linkage is to utilize the heteronuclear three-bond coupling constants, $^{3}J_{CH}$, that can subsequently be interpreted using a Karplus-type relationship to provide further information on the three-dimensional structure.

An additional source of information is attainable from NMR residual dipolar couplings (RDCs), which can be obtained when the molecule is dissolved in an orienting medium of low order. Importantly, high-resolution NMR spectroscopy techniques can then still be used.[5,6] To date, a large number of orienting media have been described that are suitable for different molecules or miscellaneous experimental conditions, including alkyl sulfates/the corresponding alcohol/sodium sulfate/water,[7] dimyristoylphosphatidylcholine (DMPC)/dihexanoylphosphatidylcholine (DHPC)/water,[8,9] di-*O*-dodecyl-*sn*-glycero-3-phosphocholine (DIODPC)/3-[(3-cholamidopropyl)dimethylammonio]-2-hydroxy-1-propanesulfonate (CHAPSO)/water,[10] $H_3Sb_3P_2O_4$ in D_2O,[11] and cetylpyridinium bromide/hexanol/sodium bromide/water.[12] The resulting information from RDCs is important, for example, in studies of peptide and protein dynamics.[13−18]

Already during the 1980s, Prestegard and co-workers were exploring orientational and conformational preferences of mono- and disaccharides in membranelike environments using either potassium laurate micelle systems or the more bilayerlike cesium perfluorooctanoate micelles.[19−22] In particular, NMR deuterium quadrupolar splittings of labeled carbohydrates were used to interpret experimental observations; both molecular orientation and conformation were adjusted in the search procedure. For

Received: February 21, 2011
Revised: April 15, 2011
Published: May 05, 2011

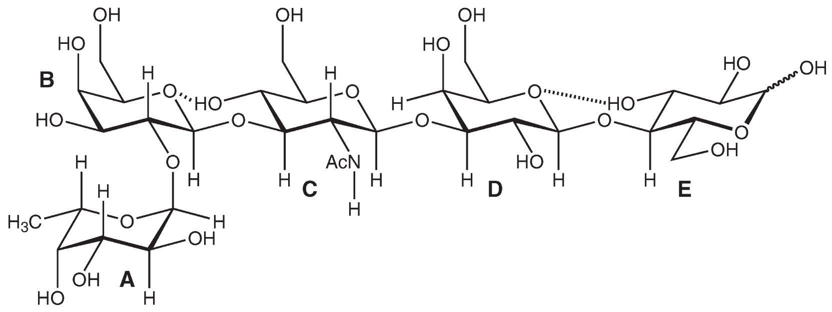

Figure 1. Schematic of the pentasaccharide lacto-*N*-fucopentaose (LNF-1), α-L-Fuc*p*-(1 → 2)-β-D-Gal*p*-(1 → 3)-β-D-Glc*p*NAc-(1 → 3)-β-D-Gal*p*-(1 → 4)-D-Glc*p*. Sugar residues are labeled A−E, starting from the terminal nonreducing end. In the text a subscript (ϕ_i, ψ_i, where i = A, B, C, D) is used to refer to the pertinent glycosidic torsion angle. Hydrogen bonds between O5 in B and HO4 in C and between O5 in D and HO3 in E revealed in the MD simulations are denoted by dashed lines.

organic molecules in general[23] and carbohydrates in particular, RDCs are a source of additional NMR observables that add knowledge about various conformational processes occurring in solution.[24−31]

Of the over 100 lactose-derived oligosaccharides found in human milk,[32,33] (1 → 2)-linked fucosyl oligosaccharides are particularly important for infants as protection against diarrhea.[34] The soluble human milk oligosaccharides are analogues to glycoconjugates on human cells and can act as decoy receptors to invading bacteria, thereby preventing bacterial adhesion to the epithelial cell surfaces that line and protect organs.[34−36] The pentasaccharide lacto-*N*-fucopentaose (LNF-1, Figure 1) has previously been investigated by ^{1}H and ^{13}C NMR spectroscopy, where chemical shifts,[37] proton−carbon long-range correlations,[38] ^{1}H,^{1}H nuclear Overhauser effects (NOEs),[39,40] and ^{13}C nuclear spin relaxation[41] experiments have been carried out. More recently, one-bond ^{1}H,^{13}C RDCs[42,43] together with molecular modeling techniques including molecular dynamics (MD) simulations[44,45] were reported. In the present study, we analyze in detail the conformational dynamics of LNF-1 using ^{1}H,^{1}H transverse rotating-frame Overhauser effect (T-ROE) experiments, trans-glycosidic $^3J_{CH}$, ^{1}H,^{13}C and ^{1}H,^{1}H RDCs, together with MD simulations of the pentasaccharide with explicit water. The combined results show a system in which several motional processes occur on various time scales and result in different conformational states for the pentasaccharide in solution.

■ MATERIALS AND METHODS

General Considerations. Lacto-*N*-fucopentaose (LNF-1) was obtained from IsoSep AB (Tullinge, Sweden). The materials for the dilute liquid-crystal solution, ditetradecylphosphatidylcholine (ditetradecyl-PC) and dihexylphosphatidylcholine (dihexyl-PC) were purchased from Avanti Polar Lipids (Alabaster, AL), and the amphiphile *N*-cetyl-*N*,*N*,*N*-trimethylammonium bromide (CTAB) was obtained from Merck (Darmstadt, Germany), all with purity > 99%. The chemicals were used without further purification. The torsion angles in LNF-1 across the glycosidic linkages are defined as follows: ϕ_A = H1A−C1A−O2B−C2B, ψ_A = C1A−O2B−C2B−H2B, and so on. Associated with the ψ_C torsion angle, C1C−O3D−C3D−H3D, the two conformational states are referred to as $\psi_C^+ > 0°$ and $\psi_C^- < 0°$.

NMR Spectroscopy. NMR experiments were performed on Varian Inova spectrometers equipped with 5-mm pulsed-field-gradient (PFG) triple-resonance probes, unless otherwise stated, at 14.1 and 18.8 T corresponding to ^{1}H frequencies of 600 and 800 MHz, respectively. Proton−proton cross-relaxation rates in LNF-1 (100 mM) were measured in D_2O solution at 25 °C using one-dimensional ^{1}H,^{1}H double-pulsed-field-gradient-spin-echo (DPFGSE) transverse rotating-frame Overhauser effect spectroscopy (T-ROESY) and two-dimensional ^{1}H,^{1}H T-ROESY experiments at 600 MHz.[46,47] Selective excitations were enabled using 35−15-Hz broad i-Snob-2 shaped pulses[48] of 49−113-ms duration. The DPFGSE part was followed by a T-ROESY spin lock with $\gamma B_1/2\pi$ = 2.9 kHz. Six different ^{1}H,^{1}H cross-relaxation delays (mixing times) between 50 and 300 ms were used. The errors in the derived distances are estimated to be less than 0.2 Å.

Measurements of the trans-glycosidic carbon−proton coupling constants were performed at 25 °C as Hadamard-4 excitation profiles using a 50-ms half-Gaussian shaped pulse, with a pulsed-field-gradient version of the pulse sequence.[49] The delay for evolution of the heteronuclear couplings was set to 30 ms employing 12640 transients in each of the two experiments. Eight times zero-filling and multiplication of the free induction decay (FID) with a 0.3-Hz exponential broadening factor were applied prior to the Fourier transformation. Coupling constants were extracted by the *J*-doubling procedure, using eight delta functions in the frequency domain. The errors in the $^3J_{CH}$ values are estimated to be less than 0.2 Hz. In addition, *J*-resolved heteronuclear multiple bond correlation (J-HMBC) experiments[50] were performed at 25 °C on Bruker Avance 500 and Bruker Avance III 700 spectrometers equipped with 5-mm cryoprobes. To avoid spectral overlap, three different scaling factors, namely, κ = 4.6, 20.6, and 24.5, calculated from $\kappa = \Delta/t_1^{max}$, where Δ was at least 60% of the inverse of the smallest coupling constant to be measured, were used to scale the coupling in the indirect (F_1) dimension. For the heteronuclear coupling constant related to the ϕ_B torsion angle, the average value was calculated from two different experiments with different scaling factors. The J-HMBC spectra were processed in magnitude mode, and coupling constants were extracted from one-dimensional projections of the resonances of interest.

The liquid-crystalline phase was prepared from two stock solutions containing ditetradecyl-PC/CTAB (30:1) and dihexyl-PC in D_2O containing 10 mM phosphate buffer (pD_c = 7.4), both with a lipid concentration of 5% w/v. After sonication, the solutions were mixed to give a ditetradecyl-PC/dihexyl-PC molar ratio of 30:10, determined by integration of the peaks in the ^{31}P NMR spectrum at 35 °C. The sample homogeneity was ensured by several cycles of cooling (0 °C), sonication, and heating (40 °C) and checked by ^{2}H NMR spectroscopy. Subsequently, 20 mg of LNF-1 was dissolved in 0.6 mL of the liquid-crystalline

solvent to give a sugar concentration of 40 mM. The resulting ^{2}H quadrupolar splitting was 19 Hz.

Proton−carbon residual dipolar couplings (d_{CH}) were obtained at 35 °C as the half-difference between the one-bond ^{1}H,^{13}C splitting measured in the ordered phase and the isotropic phase. The *J*-modulated constant-time heteronuclear single quantum coherence (CT-HSQC) experiment[51] was used with only a single pulsed-field gradient within the reverse INEPT (insensitive nuclei enhanced by polarization transfer) part of the pulse sequence. In total, six experiments with $2(T - \Delta)$ values between 18 and 28 ms were carried out for ∼10−14 h per experiment. Each spectrum consisted of 4096 or 8192 × 128 complex data points with 80−96 transients per t_1 increment and spectral widths of 3600 or 4796 and 10600 Hz in the F_2 and F_1 dimensions, respectively. The FIDs were zero-filled eight times in each dimension and multiplied by a Gaussian weighting function prior to the Fourier transformation. Cross-peak integration was performed using the same integration limits in all spectra. The couplings were obtained by fitting the cross-peak intensities from a series of experiments with different $2(T - \Delta)$ values to $C \cos[2\pi^1 J_{C,H}(T - \Delta)]$. The error in each measured coupling was estimated to be less than 0.2 Hz.

Proton−proton scalar ($^3J_{HH}$) and residual dipolar couplings (d_{HH}) of LNF-1 were obtained at 35 °C from phase-sensitive correlation spectroscopy (COSY) spectra using the NMRPipe[52] based fitting program, Amplitude-Constrained Multiple Evaluation (ACME).[53] From the splittings in the spectra, J and $J + 2d$ were obtained for LNF-1 in the isotropic phase and in the ordered phase, respectively. In the experiments, 32 transients were acquired for each of the 128 t_1 increments using a relaxation delay between the scans of $>5T_1$. At 800 MHz, the signed COSY experiment[54] with a ^{1}H,^{1}H TOCSY mixing time of 40 ms was performed on LNF-1 in the ordered phase with 256 transients per t_1 increment. The errors in the measured couplings are estimated to be less than 0.3 Hz.

The ^{13}C NMR assignments for the hydroxymethyl groups of residues B−D in LNF-1[37] were revised, resulting in shifts of 61.92, 61.63, and 61.76 ppm for residues B, C, and D, respectively. Consequently, the ^{13}C relaxation data for the hydroxymethyl groups given in Table 1 of ref 41 should be changed from B6 to D6, from C6 to B6, and from D6 to C6 (i.e., C6 differs significantly from B6 and D6).

Molecular Simulations. For the molecular dynamics (MD) simulations, chemistry at Harvard macromolecular mechanics (CHARMM)[55] (parallel version, C27b4) software was used employing a CHARMM22 type of force field[56] modified for carbohydrates and referred to as PARM22/SU01.[57] Initial conditions were prepared by placing LNF-1 (α-anomeric form) in a previously equilibrated cubic water box of length 40.39 Å containing 2197 modified TIP3P (three-site transferable intermolecular potential) water[58] molecules and removing the solvent molecules that were closer than 2.5 Å to any solute atom. This procedure resulted in a system with LNF-1 and 2124 water molecules. Energy minimization was performed with steepest descent, 200 steps, followed by adopted basis Newton−Raphson until the root-mean-square gradient was less than 0.01 kcal mol^{-1} Å^{-1}. The simulation was carried out with the leapfrog algorithm,[59] a dielectric constant of unity, and a time step of 2 fs, and data were saved every 0.2 ps for analysis. SHAKE was used to restrain hydrogen−heavy atom bonds[60] with a tolerance gradient of 10^{-4}. Using different initial conditions, four separate simulations were carried out. The initial velocities were assigned at 103 K, followed by heating in 5 K increments for 8 ps to 303 K, where the system was equilibrated for 200 ps. The production runs were performed for 5, 5, 14, and 18 ns, with the temperature scaled by Berendsen's weak coupling thermostat.[61] Periodic boundary conditions and the minimum image convention were used. An atom-based force-shift method[62] with a spherical cutoff acting to 12 Å was used to truncate long-range electrostatic interactions. For the van der Waals interactions, an atom-based shifting function with a spherical radius of 12 Å was employed to truncate the nonbonded interactions. The nonbond list was generated to 13 Å and updated every 10 steps. In analysis of averages, equilibrium properties, and relaxation times, the full 42 ns of simulation data was used.

Simulations were performed on an HP Itanium2 Cluster computer at the Center for Parallel Computers, KTH, Stockholm, Sweden, using eight nodes with two processors per node, resulting in a CPU time of approximately 44 h per nanosecond.

RESULTS AND DISCUSSION

Analysis of NMR Residual Dipolar Couplings. The description of the orientational order of LNF-1 can be carried out by utilizing information from RDCs obtained in orienting media. In the present investigation, we chose the lyotropic liquid-crystalline phase prepared from ditetradecyl-PC/dihexyl-PC/CTAB because it is more stable than the corresponding ester-based DMPC/DHPC mixture. The ordered phase was assessed from the presence of two peaks of equal intensity, the peak separation of which is equal to the residual quadrupolar coupling of D_2O observed for the preparation.[63]

One-bond ^{1}H,^{13}C RDCs are readily measured because the $^1J_{CH}$ values are large, ∼150 Hz, and the ordering induced by the liquid-crystal phase results in RDCs that are an order of magnitude smaller. The $^1J_{CH}$ and $^1J_{CH} + 2d_{CH}$ values were measured in the isotropic and ordered phases, respectively, using a *J*-modulated CT-HSQC experiment. It was possible to extract the one-bond RDCs for most CH pairs of LNF-1 (Table 1). With five RDCs per rigid fragment, one can at best determine the alignment tensor for each sugar residue (assuming that none of the almost-parallel CH bond vectors are redundant). The procedure can indicate whether the oligosaccharide is rigid or not; specifically, if the alignment tensors of the different sugar residues are significantly different, the oligosaccharide is flexible. However, the reverse is not necessarily true. To obtain additional information, we turned to homonuclear ^{1}H,^{1}H RDCs obtained from analysis of a ^{1}H,^{1}H COSY spectrum by the ACME procedure. Despite the absence of *J* couplings, it is possible to extract the magnitudes of d_{HH} values, but not the sign of the RDCs. However, because the magnitudes of $^3J_{HH}$ for the intraresidue correlations are known from the ^{1}H NMR spectrum and the ^{1}H,^{1}H COSY spectrum and their signs are assumed to be positive for the three-bond coupling constants, we were able to obtain valuable information by combining the data with those from a ^{1}H,^{1}H signed COSY spectrum, which herein used total correlation spectroscopy (TOCSY) transfer as part of the experiment (Figure 2a). The two homonuclear correlated experiments are different, and not all cross-peaks are observed in both spectra. In some cases, just two possibilities exist including sign and magnitude (e.g., H1D−H2D), but in other cases, only the (relative) sign is obtained (e.g., H1D−H3D; Table 1).

The through-space magnetic dipolar coupling between spins i and j, with magnetogyric ratios γ_i and γ_j, is given

Table 1. Residual Dipolar Couplings (in Hz) for LNF-1 in a Ditetradecyl-PC:Dihexyl-PC:CTAB Ordered Phase

heteronuclear atom pair	expt	calc	homonuclear atom pair	expt	calc	relative sign of $J + 2d_{HH}$
H1A−C1A	−5.6	−5.6	H1A−H2A	−5.2/1.0	1.0	1[a]
H2A−C2A	−2.0	−2.0	H2A−H3A		−1.0	1
H3A−C3A	−2.0	−2.0	H5A−H6A		0.2	1
H4A−C4A	−5.6	−5.6	H1B−H2B	−7.3/−0.4	−0.4	1
H5A−C5A	−0.7	−0.7	H1B−H3B		−0.5	0
H1B−C1B	1.2	1.2	H2B−H3B		0.7	1
H2B−C2B	2.3	2.3	H1C−H2C	−9.2/0.7	0.2	1
H3B−C3B	2.2	2.2	H1C−H3C		−0.6	0[b]
H4B−C4B	1.9	1.9	H1C−H3D	−3.5/3.5	−0.7	nd[c]
H1C−C1C	3.3	3.3	H2C−H3C		0.8	1
H2C−C2C	4.1	4.1	H3C−H4C		0.4	1
H3C−C3C	4.5	4.5	H4C−H5C		0.0	1
H4C−C4C	3.0	3.0	H1D−H2D	−7.5/−0.5	−0.5	1
H5C−C5C	3.4	3.4	H1D−H3D		−0.9	0
H1D−C1D	3.3	3.3	H2D−H3D		1.0	1
H2D−C2D	4.4	4.4	$H1E_\alpha$−$H2E_\alpha$	−5.1[d]/1.3[d]	1.3	1
H3D−C3D	5.0	5.0	$H4E_\alpha$−$H5E_\alpha$		0.9	1
H4D−C4D	1.9	1.9	$H1E_\beta$−$H2E_\beta$	−8.2[d]/0.4[d]	0.6	1
$H1E_\alpha$−$C1E_\alpha$	−6.3	−6.3	$H2E_\beta$−$H3E_\beta$	−7.3[d]/−1.5[d]	0.2	1
$H2E_\alpha$−$C2E_\alpha$	1.8	1.8	$H4E_\beta$−$H5E_\beta$		0.3	1
$H3E_\alpha$−$C3E_\alpha$	2.0	2.0				
$H5E_\alpha$−$C5E_\alpha$	2.2	2.2				
$H1E_\beta$−$C1E_\beta$	1.1	1.1				
$H2E_\beta$−$C2E_\beta$	1.1	1.1				

[a] Arbitrary phase of the cross-peak in the signed COSY spectrum related to $J + 2d_{HH}$. [b] Opposite phase of the cross-peak in the signed COSY spectrum related to $J + 2d_{HH}$. [c] nd = not determined. [d] Results from the phase-sensitive $^1H,^1H$ COSY experiments analyzed by ACME were interpreted for the subsequent analysis of LNF-1 as if only the pertinent anomeric form was present in solution, based on the ratio between the α- and β-anomeric forms of 36:64.

(in Hz) by[64]

$$d_{ij} = -\frac{\mu_0}{8\pi^2}\frac{\gamma_i\gamma_j\hbar}{2}\langle(3\cos^2\theta_{ij} - 1)r_{ij}^{-3}\rangle \quad (1)$$

where θ_{ij} is the angle between the spin−spin vector and the external magnetic field and r_{ij} is the spin−spin distance. The angular bracket denotes that the RDCs are averaged over both molecular tumbling and internal bond rotations. To determine the orientation of the relevant vectors (C−H or H−H) in the molecular frame, eq 1 is written to contain three successive rotations: θ_{ij}^{α} are the angles between the spin−spin vector and the α axis in molecular coordinate frame. The order parameters, $S_{\alpha\beta}$, that are elements of the order matrix **S**, describe the second rotation, namely, the average orientation of the molecular axis system relative the liquid-crystal director. Finally, the angle β defines the orientation of the director with respect to the magnetic field (β = 90°). Thus, the observed residual dipolar coupling can be expressed as

$$\begin{aligned} d_{ij} = \frac{b_{ij}}{4}[&S_{zz}(3\cos^2\theta_{ij}^z - 1) + (S_{xx} - S_{yy})(\cos^2\theta_{ij}^x - \cos^2\theta_{ij}^y) \\ &+ 4S_{xy}\cos\theta_{ij}^x\cos\theta_{ij}^y + 4S_{xz}\cos\theta_{ij}^x\cos\theta_{ij}^z \\ &+ 4S_{yz}\cos\theta_{ij}^y\cos\theta_{ij}^z](3\cos^2\beta - 1) \end{aligned} \quad (2)$$

where the dipole−dipole coupling constant is given by $b_{ij} = -\mu_0\gamma_i\gamma_j\hbar/8\pi^2 r_{ij}^3$.

We start the analysis by considering the orientational order in the five rigid fragments (sugar rings) of LNF-1. This order is determined from the conformation-independent homonuclear, d_{HH}, and heteronuclear, d_{CH}, dipolar couplings collected in Table 1. In the table, calculated dipolar couplings are included for all five fragments, and these are in good agreement with the experimental values. In principle, all dipolar couplings are conformation-dependent, because each conformational state corresponds to its own order tensor. Here, we consider only dipolar couplings that do not change the distance upon conformational transition. The order tensor in each rigid sugar residue of LNF-1 consists of five order parameters; thus, (at least) five linearly independent dipolar couplings are required for complete determination of this tensor. Comparison of the entire tensor for these fragments can therefore be complicated. Fortunately, there is a convenient scalar parameter that characterizes the molecular ordering,[6,65] which is called the generalized degree of order (GDO), ϑ^R

$$\vartheta^R = \sqrt{\frac{2}{3}\sum_{a,b=x,y,z}(S_{ab}^R)^2} \quad (3)$$

where S_{ab}^R are the order parameters (eq 2) determined for the rigid fragment R, where R = {A, B, C, D, E}. The values for the GDOs in the rigid units of LNF-1 are collected in Table 2. Clearly, the GDOs calculated using a single energy-minimized structure exhibit significant variations and very large error limits. The reason for these large uncertainties is that several C−H

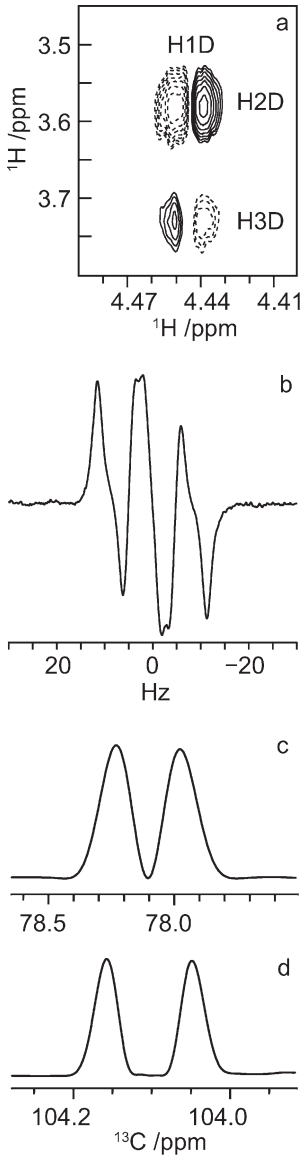

Figure 2. (a) Part of the ^{1}H,^{1}H signed COSY NMR spectrum of LNF-1 in the ordered phase showing different phases of the cross-peaks in residue D (dashed lines = negative intensity, solid lines = positive intensity). (b) The H2 resonance of residue B in LNF-1 after selective excitation of the C1 resonance in residue A to detect the trans-glycosidic $^3J_{CH}$ coupling. Selected one-dimensional projections from a ^{1}H,^{13}C J-HMBC NMR spectrum of LNF-1 recorded with the scaling factor (c) κ = 20.6 showing the peak separation for $\kappa^3J_{H1B,C3C}$ and (d) κ = 4.6 showing the peak separation for $\kappa^3J_{H3D,C1C}$.

vectors relevant for experimental d_{CH} values in all sugar units are nearly parallel; thus, the dipolar couplings are not linearly independent. In particular, in unit D, four of five vectors are essentially parallel. By including several frames from the trajectory generated in the MD simulation (vide infra), this linear dependence is removed, resulting in significantly smaller errors. This effect is observed for 10 frames and only slightly enhanced by using 1000 frames. The GDOs obtained in the analysis with several frames indicate remarkably similar ordering for all units R = {A, B, C, D, E}. To a first approximation, this can be interpreted as LNF-1 being a cylinder where most of the C−H vectors are oriented perpendicular to the symmetry axis of the cylinder.

Table 2. Generalized Degree of Order (GDO), ϑ^R, Determined from the Dipolar Couplings within Rigid Fragments (Hexopyranose Ring) of LNF-1

	ϑ^R		
fragment (R)	minimum-energy frame	10 frames	1000 frames
A	69 ± 9[a]	66 ± 4	64 ± 3
B	139 ± 76	61 ± 31	56 ± 23
C	460 ± 200	54 ± 5	50 ± 4
D	221 ± 78	95 ± 39	80 ± 26
E	99 ± 35	65 ± 5	62 ± 5

[a] Values were multiplied by a common factor (10^5), and error limits are related to the experimental dipolar couplings.

In fact, the H1E$_\alpha$−C1E$_\alpha$ dipolar coupling that is close to parallel to the symmetry axis clearly exhibits the largest magnitude among the C−H couplings in this fragment. The fact that the local order of all of the sugar units is similar does not imply that conformational motion in the molecule is absent.

For the analysis of the conformational behavior of LNF-1, only one trans-glycosidic RDC could be determined, $d_{H1C,H3D}$, under the experimental conditions. Using the conformational distribution functions determined from the heteronuclear spin−spin coupling constants and homonuclear T-ROE parameters (vide infra), together with the order tensors for units C and D, we were able to calculate this coupling to be −0.7 Hz, compared to the experimental value of either −3.5 Hz or +3.5 Hz. The error limits of the calculated coupling are very large (±13 Hz), and in this case, a conclusive result regarding the observed trans-glycosidic RDC was not possible. However, the results of the signed COSY experiment (Table 1) were in complete agreement with the model of LNF-1 (vide infra).

Conformational Analysis Using MD Simulations. Molecular dynamics simulations of LNF-1 were performed in the isotropic phase with explicit water as the solvent. A modified CHARMM force field referred to as PARM22/SU01 was employed[57] in the simulations with a total production time of 42 ns. At three of the glycosidic linkages, between pairs of residues A−B, B−C, and D−E, a major conformational state was present, with some small and relatively short excursions to other nearby regions (Figure 3). However, at the glycosidic linkage between residues C and D, two interconverting states are present as a result of flexibility at the ψ_C torsion angle. These conformational states are referred to as $\psi_C^+ > 0°$ and $\psi_C^- < 0°$ and were populated to 48% and 52%, respectively, with $\langle\psi_C^+\rangle = 39°$ and $\langle\psi_C^-\rangle = -40°$. Selected torsion angle averages from the MD simulation are compiled in Table 3, and the trajectories for several conformational parameters are shown in Figure 4. The conformations at the ϕ glycosidic torsion angles are in agreement with those anticipated from the presence of an exo-anomeric effect.[66] Thus, all ϕ torsion angles populate essentially a single state and show a root-mean-square deviation (rmsd) of ∼15°, whereas the corresponding rmsd for the ψ_C torsion angle is about 3 times larger as a result of the transition processes.

In one of the earlier studies on LNF-1,[40] the conformational preference of the *N*-acetyl group of residue C was investigated. A large $^3J_{HN,H2}$ value of 10.2 Hz indicated a trans relationship for the τ_H torsion angle and, together with the NOEs from the HN proton to H1 in residue B and H3 in residue C, a preference of the τ torsion angle for a value of 60° ± 30°. The results from the present MD simulations (Figure 5) for the *N*-acetyl group in

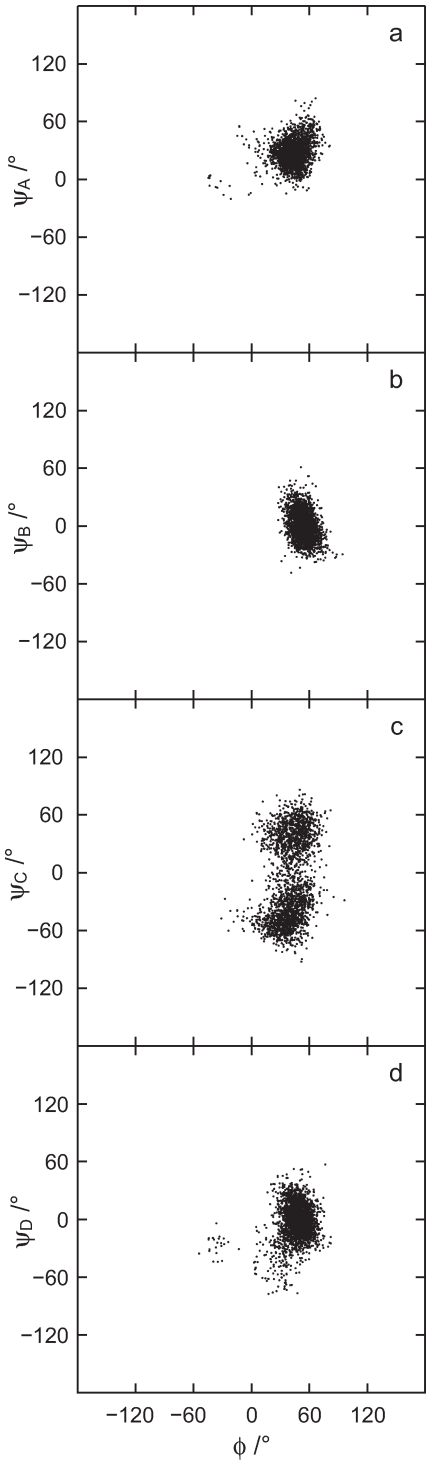

Figure 3. Scatter plots of ϕ versus ψ from the 14-ns MD simulation of LNF-1 showing the (a) (1 → 2) linkage between residues A and B, (b) (1 → 3) linkage between B and C, (c) (1 → 3) linkage between C and D, and (d) (1 → 4) linkage between D and E.

LNF-1 are consistent with the previously reported[40] experimental data. We observe (i) a large calculated $^3J_{HN,H2}$ value, (ii) short effective distances for HNC−H1B (2.53 Å) and HNC−H3C (2.43 Å), and (iii) a longer HNC−H1C distance (2.71 Å). Most interestingly, during the MD simulation, a transition occurs at the τ_H torsion angle to an s-cis conformation lasting for ~1 ns, before

Table 3. Averages Calculated from the Trajectory Generated in the MD Simulation of LNF-1 and Experimental $^3J_{CH}$ Values

torsion angle (deg)		$^3J_{CH}$ (Hz)	
ϕ_A	43 (13)[a]	$J_{\phi A}$	3.4[b] [3.4][c]
ψ_A	28 (14)	$J_{\psi A}$	4.9 [5.5]
ϕ_B	54 (9)	$J_{\phi B}$	2.2 [2.0][d]
ψ_B	1 (15)	$J_{\psi B}$	6.2 [5.0]
ϕ_C	42 (15)	$J_{\phi C}$	3.5 [4.0]
ψ_C	−2 (43)	$J_{\psi C}$	3.7 [4.2][d]
ϕ_D	47 (13)	$J_{\phi D}$	2.9 [3.6]
ψ_D	−2 (19)	$J_{\psi D}$	6.0 [nd][e]
τ_H	157 (34)		
τ	92 (32)		

[a] Root-mean-square deviations in parentheses. [b] Calculated from MD simulations and Karplus-type relationship described by Cloran et al.[77] [c] Experimental values in square brackets. [d] Experimental values determined using the J-HMBC technique. [e] nd = not determined.

it returns to the s-trans conformation. During this time course, the fucosyl group (residue A) enters another conformational state in which both ϕ_A and ψ_A are altered. The transition back to the exo-anomeric conformation occurs prior to the transition of the *N*-acetyl group. An analysis of the above-described effective distances involving the HNC proton shows that, in the s-cis conformation, they are all longer by approximately 1 Å, which suggests that the s-cis conformation is present to only a small extent. These results indicate that the *N*-acetyl group acts as a switch in allowing the fucosyl group to enter into a changed conformational state and an altered three-dimensional shape of the molecule.

From the MD simulations, we note that the transitions at torsion angle ψ_C of the β-(1 → 3) linkage between residues C and D occur on a subnanosecond time scale. Previously, we used NMR spin relaxation experiments to determine the overall rotational diffusion of LNF-1 as slightly anisotropic with a prolate shape and a global reorientational correlation time for τ_M of ~0.6 ns.[41] The rapid internal motions were determined to be an order of magnitude faster, with $\tau_e \approx 60$ ps. To quantify the transition process at the ψ_C torsion angle, we identify the two states ψ_C^+ and ψ_C^- with transitions between the wells as for a bistable potential. Furthermore, N_+ and N_- are defined as populations ($N_+ + N_- = 1$) in the wells, and k_+ and k_- are the rate constants for the transition process. To investigate the transition rates, a number correlation function, $C_N(t)$, can be defined, where each state along a trajectory is identified as unity if the molecule has the conformation of the reactant well and zero if it is in the product well.[67,68] The relaxation time of $C_N(t)$ is related to the rate constant as follows

$$\tau_N = (k_+ + k_-)^{-1} \quad (4)$$

where the rate constant k_+ can be written as

$$k_+ = (1.0 - \langle N_+ \rangle)/\tau_N \quad (5)$$

From the MD simulations, a number correlation function was calculated for the isomerization process at the ψ_C torsion angle (Figure 6). Fitting the decay between 10 and 110 ps to a monoexponential function gave τ_N = 101.5 ps. Using $\langle N_- \rangle$ = 0.5205, the following rate constants were subsequently obtained: $k_+ = 4.75\ ns^{-1}$ and $k_- = 5.15\ ns^{-1}$. The standard deviations in the rates, estimated from $(2\tau_N/T)^{1/2}$, where T is the length of the

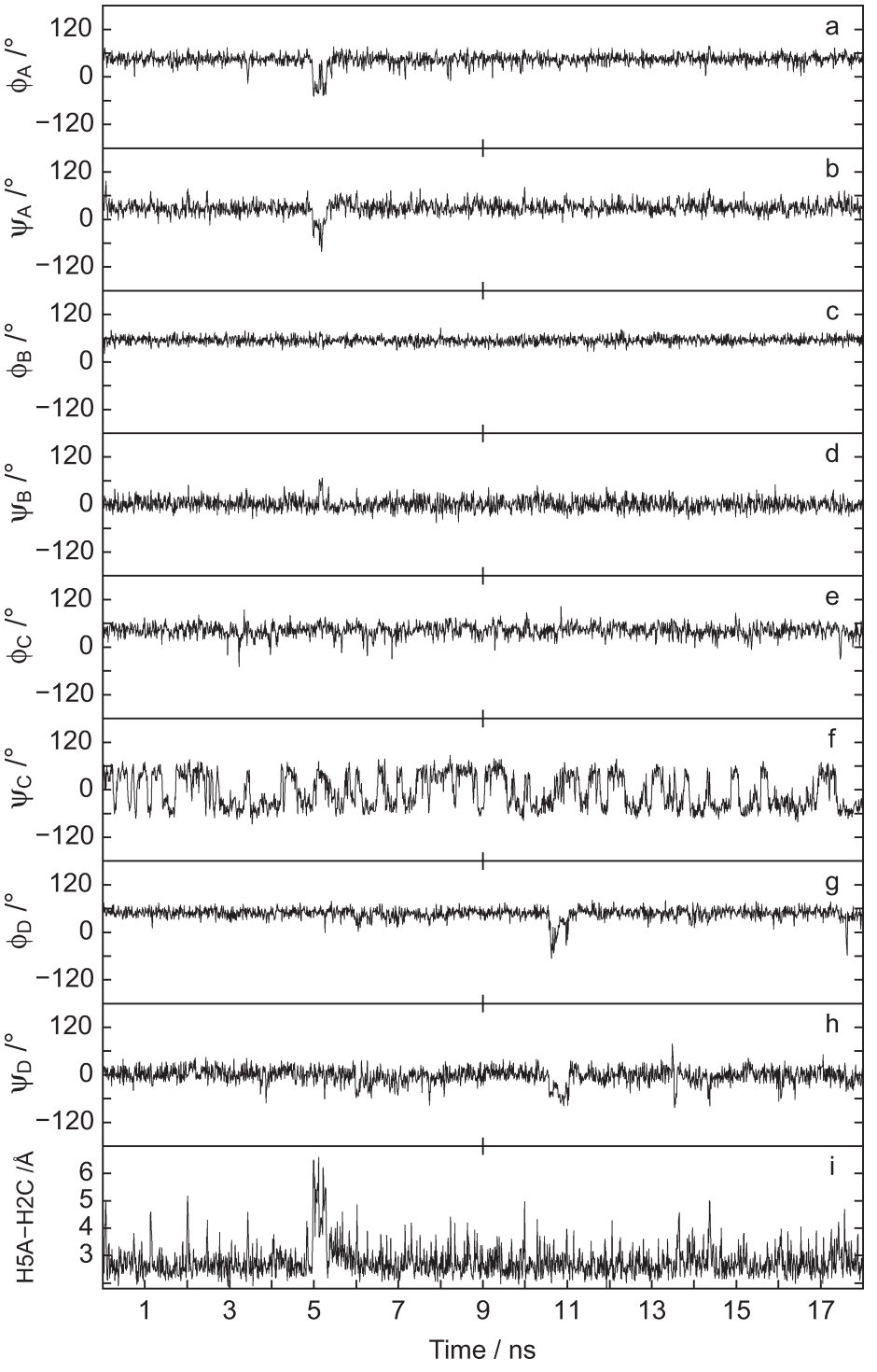

Figure 4. Time dependence of the (a−h) glycosidic torsion angles of LNF-1 from the 18-ns MD simulation and (i) inter-residue proton−proton distance between H5 in residue A and H2 in residue C.

trajectory,[68,69] are 0.07, and the standard deviations in the populations, estimated from $(\tau_N/2T)^{1/2}$,[68] are 0.035. Thus, from the MD simulations, we note that the transitions take place on a subnanosecond time scale and the conformational states ψ_C^+ and ψ_C^- are equally populated.

To compare the simulation results to experimental data, we have to consider the following aspects: The viscosity of the TIP3P water model used at 303 K employing spherical boundary conditions and truncation of long-range interactions is lower[70,71] than that for pure water by a factor of ∼0.7, and the experimental NMR data were acquired in D_2O instead of H_2O, where η_{H_2O}/η_{D_2O} = 1.23.[72] Thus, the difference in viscosity between the experimental NMR conditions and the MD simulation model is a factor of ∼1.75. The effect of viscosity on the kinetics and rate processes often depends inversely to the first power, but for some processes, a fractional viscosity dependence has been observed in

dx.doi.org/10.1021/jp2017105 |J. Phys. Chem. B 2011, 115, 7109–7121

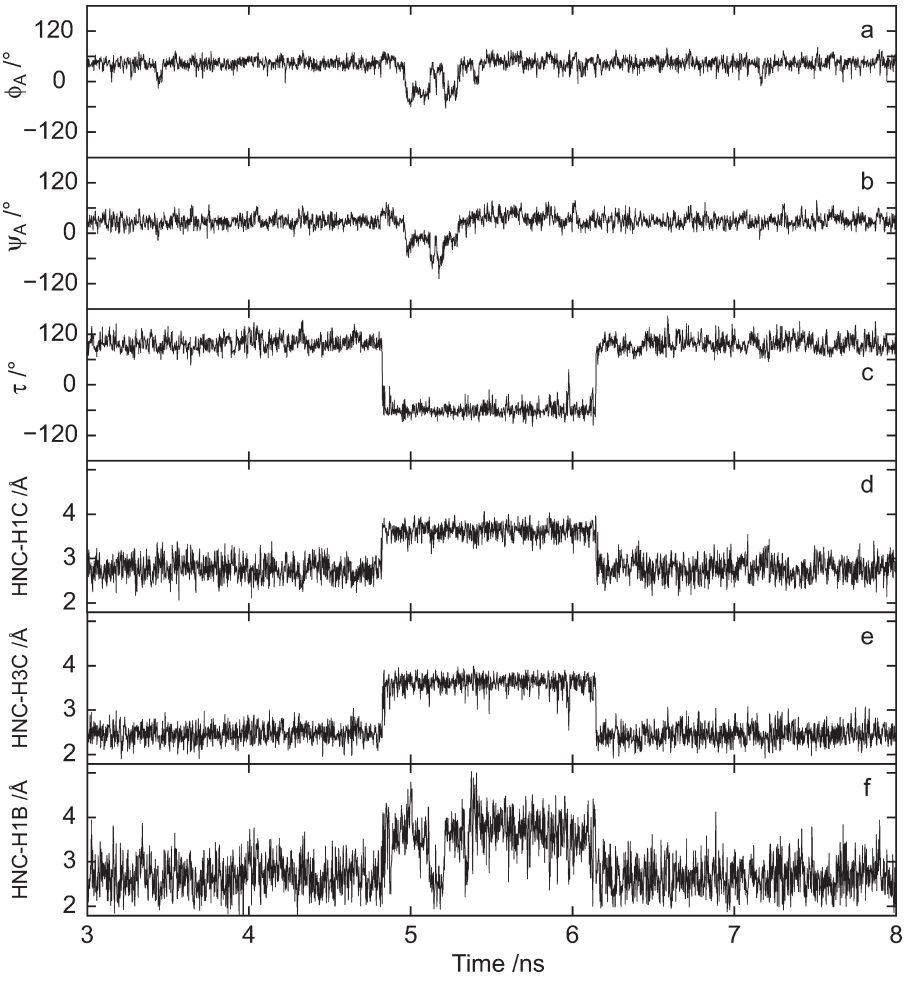

Figure 5. Selected time region from the 18-ns MD simulation of LNF-1 for the (a,b) glycosidic torsion angles of residue A, (c) torsion angle of the *N*-acetyl group, and (d−f) proton−proton distances between the HN proton and selected protons in residues C and B.

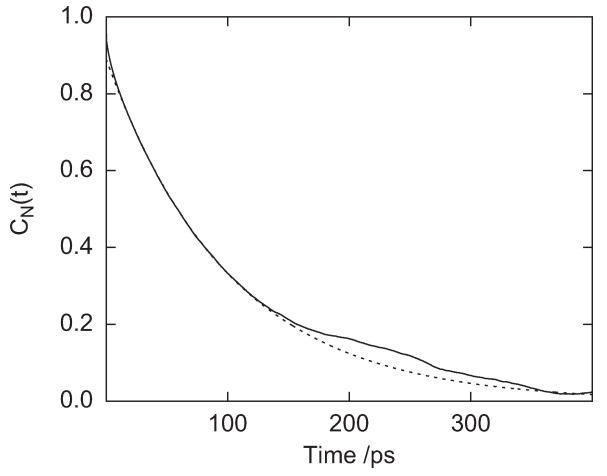

Figure 6. Number correlation function, $C_N(t)$, for the isomerization process at the glycosidic torsion angle ψ_C. The dashed line shows a monoexponential decay with a time constant of τ = 101 ps as obtained from the fit to $C_N(t)$ between 10 and 110 ps.

which the rate varies as $\eta^{-\alpha}$, where $\alpha \approx 0.6$.[73] Scaling to the experimental conditions using simply η^{-1}, we obtain: $k_{+(\text{scaled})} \approx 2.7\ \text{ns}^{-1}$ and $k_{-(\text{scaled})} \approx 2.9\ \text{ns}^{-1}$. Consequently, $\tau_{N(\text{scaled})} \approx 0.18$ ns. Thus, the time constant for the isomerization relaxation process is indeed shorter than the global reorientation time, as $\tau_M \approx 0.6$ ns from ^{13}C NMR relaxation data.[41] However, this might make the interpretation of the ^{13}C relaxation data difficult, and alternative approaches to the interpretation of NMR relaxation data when coupled motions are present might be preferable.[74]

The presence of intramolecular hydrogen bonds can be analyzed from the MD simulation using geometric criteria: a hydrogen bond is present if the distance between the hydrogen atom and the acceptor atom is <2.5 Å and the donor−hydrogen−acceptor angle is >135°. In LNF-1, a previous hydrogen-bond analysis[43] from an MD simulation revealed the presence of hydrogen bonds, for example, between O5 in B and HO4 in C, as well as between O5 in D and HO3 in E. These hydrogen bonds were also present herein to significant extents, namely, 29% and 28% of the MD trajectory. Thus, based on the predictions from the molecular simulation using an all-atom-based force-field approach, hydrogen bonding between the sugar residues might be an important factor stabilizing well-defined structures or structural elements. However, the transglycosidic hydrogen bond in methyl α-cellobioside between the HO3 group of the reducing-end α-D-Glc*p* residue and the O5 ring oxygen in the terminal *β*-D-Glc*p* group (cf. residues D and E in LNF-1) could not be confirmed using the ^{13}C site-specifically labeled isotopologue *β*-D-[4-^{13}C]Glc*p*-(1 → 4)-α-D-Glc*p*-OMe.[75]

dx.doi.org/10.1021/jp2017105 |*J. Phys. Chem. B* 2011, 115, 7109–7121

Table 4. Effective Proton−Proton Distances *r* for LNF-1 Calculated from the MD Simulation and Derived by Cross-Relaxation Rates σ from ^{1}H,^{1}H T-ROESY NMR Experiments Using ISPA

atomic interaction	MD distance (Å)[a]	NMR distance (Å)	σ (s^{-1})
H1A−H2A	2.39	2.39[b]	0.287
H1A−H2B	2.43	2.44	0.254
H1B−H3C	2.38	2.38	0.298
H1C−H3D	2.39	2.34	0.327
H1D−H4E	2.33	2.49	0.226
H1C−H2D	3.41	>3.5	<0.03
H1A−H2C	5.75	>3.5	<0.03
H3A−H5A	2.58	2.58[c]	0.140
H1C−H4D	3.13	3.62	0.018
H5A−H1B	3.59	3.31	0.031
H5A−H2B	3.09	3.15	0.043
H5A−H2C	2.52	2.56	0.147

[a] $1/r = \langle r^{-6}\rangle^{1/6}$. [b] Reference distance from MD simulation for two-dimensional ^{1}H,^{1}H T-ROESY experiments. [c] Reference distance from MD simulation for one-dimensional ^{1}H,^{1}H T-ROESY experiments.

Comparison of MD Simulations with Experimental NMR Data. The microscopic description of the conformational transitions of LNF-1 in solution from the MD simulation can be investigated by comparison to experimental data using NMR observables calculated from the MD trajectory. Karplus-type relationships[76] for analysis of trans-glycosidic torsion angles have continuously been developed, and the $^3J_{CH}$ values can therefore serve as an important indicator as to whether a simulation properly samples the conformational states of the molecule. Measuring the $^3J_{CH}$ values using selective Hadamard excitation of ^{13}C resonances offers an efficient way of acquiring the data.[49] The resulting ^{1}H-detected spectrum shows homonuclear couplings observed in-phase and the required heteronuclear couplings in antiphase (Figure 2b). Most often, the *J*-doubling procedure is used to extract the coupling constants, as partial cancellation makes it difficult to measure them directly. In addition, two-dimensional J-HMBC experiments based on scaling the coupling in the indirect (F_1) dimension (Figure 2c,d) were also employed to measure $^3J_{CH}$ coupling constants, which could not be obtained using the above-described one-dimensional NMR technique. The experimentally observed $^3J_{CH}$ values are collected in Table 3. The Karplus-type relationship derived for trans-glycosidic correlations by Cloran et al.[77] was used to calculate the $^3J_{CH}$ values from the MD trajectory. The agreement with experimental data is good to excellent for the measured coupling constants. The calculated $^3J_{CH}$ value related to the ψ_D torsion angle, however, is too large because the torsion angle is close to eclipsed in the MD simulation.

The experimental T-ROE data (Table 4) were analyzed using the isolated spin-pair approximation $r_{ij} = r_{ref}(\sigma_{ref}/\sigma_{ij})^{1/6}$, where *r* refers to a proton−proton distance and σ to the corresponding cross-relaxation rate. There is excellent agreement between the effective proton−proton distances derived from the MD trajectory and those calculated from the experiments. This is particularly interesting for the H5A−H2C distance (Figure 4i), which is dependent on two glycosidic linkages, corresponding to four torsion angles. The calculated effective distance from the MD simulation is 2.52 Å compared to the experimentally determined value of 2.56 Å, indicating that the conformation and dynamics of the trisaccharide element A−B−C are well-described by the MD simulation. The deviation at the reducing end (i.e., the H1D−H4E proton−proton distance) points to the fact that a higher flexibility is present in the molecule than observed in the MD simulation. These observations are in complete accord with those previously drawn based on ^{13}C nuclear spin relaxation studies.[41]

As a prerequisite for obtaining the one-bond d_{CH} value, the $^1J_{CH}$ coupling constants were determined in the isotropic phase and thus were readily available as parameters in the conformational analysis. A conformational dependence of the $^1J_{C1,H1}$ coupling constants on the glycosidic torsion angle ϕ was reported by Tvaroska and Taravel[78]

$$^1J_{C1,H1} = 0.57\cos 2\phi - 3.46\cos\phi + 1.63\sin 2\phi - 1.53\sin\phi + 161.5 + 0.0390\varepsilon \quad (6)$$

where ε is the dielectric permittivity and we assume $\varepsilon = 80$ for water solution. For sugar residues C and D, the experimentally determined $^1J_{C1,H1}$ coupling constants are 163.45 and 162.78 Hz, respectively. The $^1J_{C1,H1}$ values were calculated from the MD trajectory as 162.61 and 162.67 Hz for $^1J_{C1,H1}$ in residues C and D, respectively. The RMSDs are <0.2 Hz, which is also the estimated experimental error in the determination. From the MD simulations, we have $\langle\phi_C^+\rangle = 45°$ and $\langle\phi_C^-\rangle = 39°$, and the calculated $^1J_{C1,H1}$ values are in good agreement with the experimentally determined values, supporting the conformational preference where $\phi \approx 40°$, that is, where the exo-anomeric conformation prevails.[66] The conformational region for which the $^1J_{C1,H1}$ coupling constant is >164 Hz (i.e., between ~130° and ~280°) can consequently be disregarded as a major population region, although a minor contribution at this torsion angle region cannot be ruled out.

The pentasaccharide LNF-1 has previously been studied using different molecular simulation techniques and various NMR experiments.[42−45] Using an RDC-based approach,[42] low-energy conformations consistent with experimental data were identified. For the β-D-Glc*p*NAc-(1→3)-β-D-Gal*p* structural element, only the conformation with $\psi \approx -40°$ was found to be important. A subsequent study[43] using a Glycam-93-based force field in the MD simulation showed a narrower ψ distribution than observed using the presently employed PARM22/SU01 force field. Conformational search protocols can be used to find accessible regions in space prior to an MD simulation,[79] and in the case of LNF-1, the conformational regions that are sterically allowed and energetically accessible are always much larger than those observed in the MD simulations using explicit water molecules as the solvent.[44] A recent MD simulation of LNF-1[45] using the OPLS-AA (all-atom optimized potentials for liquid simulations) force field and the SPC (simple point charge) water model showed that the ϕ,ψ conformation space was similar to that observed herein; for example, the ψ_A distribution is somewhat narrow with positive torsion angles, as was also observed using the Glycam-93 force field. However, whereas the β-D-Glc*p*NAc-(1→3)-β-D-Gal*p* structural element can exist in two distinct conformational states,[45] it almost exclusively populates that in which the torsion angle is positive ($\psi = +57°$) using the OPLS-AA force field. In contrast to the excellent agreement for the H5A−H2C distance, where the MD simulation (OPLS-AA force field) results in an interatomic distance of 2.55 Å, that between H1C−H3D is ~3.1 Å from an MD-refined structure. The latter distance is substantially longer than that observed

herein using both MD simulations and experimental T-ROE data (Table 4). Thus, it is suggested that two significantly or almost equally populated conformational states at the ψ_C torsion angle result in a much better agreement with the experimental NMR data than a model in which either one of the two states is exclusively or predominantly populated.

Conformational Distribution Functions Utilizing Generalized Order Parameters. The molecular structure and flexibility are conveniently described using the conformational probability distributions, $P(\phi,\psi)$, where the two torsion angles, ϕ and ψ, are related to the glycosidic linkage. The major degrees of freedom and, thus, conformational transitions in oligosaccharides are dictated by the bond rotations at ϕ and ψ. The analysis is based on the maximum-entropy (ME) method,[80,81] which allows for continuous bond rotations. In the ME analysis, we used the NMR parameters determined in the isotropic phase, namely, the scalar ($^3J_\phi$ and $^3J_\psi$) couplings and the T-ROE parameters (σ, related to r^{-6}) for the determination of $P(\phi,\psi)$ as

$$P(\phi,\psi) = Z^{-1}P_{rep}(\phi,\psi)\exp\left[-\sum_{ij}\lambda_{ij}{}^3J_{ij}(\phi,\psi)-\sum_{kl}\lambda_{kl}r_{kl}^{-6}(\phi,\psi)\right] \quad (7)$$

where the adjustable parameters λ_{ij} and λ_{kl} were determined by bringing calculated scalar couplings and T-ROE parameters into agreement with experimental observables. $P_{rep}(\phi,\psi)$ accounts for possible steric repulsions in the molecule and is defined as

$$P_{rep}(\phi,\psi) = Z_{rep}{}^{-1}\exp[-U_{rep}(\phi,\psi)/k_BT] \quad (8)$$

where $U_{rep}(\phi,\psi) = \Sigma_{pq}\varepsilon_{pq}^{LJ}(r_{pq}^{LJ}/r_{pq})^{12}$, the parameters ε_{pq}^{LJ} and r_{pq}^{LJ} were taken from the CHARMM22 force field,[55] and Z and Z_{rep} are normalization factors.

Using $P(\phi,\psi)$, one can calculate the average of the NMR parameter X, with $X = \{J, \text{T-ROE}\}$, as

$$\langle X\rangle = \int X(\phi,\psi)\,P(\phi,\psi)\,d\phi\,d\psi \quad (9)$$

The strategy used in the analysis was to fit the experimental NMR parameters collected in Tables 3 and 4 to eqs 7 and 9. The distribution function $P(\phi,\psi)$ was constructed using λ_{ij} and λ_{kl} parameters. The numerical fitting of the λ parameters was performed employing a computer code written in-house, based on the MATLAB subroutine fminu.[82] The resulting distribution functions, $P(\phi,\psi)$, carry information about the populated conformational space and the extent of flexibility at the corresponding glycosidic linkage. The distribution functions for the A−B and B−C fragments turned out to be quite similar to those derived from the MD simulations (Figure 3a,b). However, the conformational distribution function derived from the J couplings and T-ROE parameters for the C−D fragment is shown in Figure 7 and exhibits three maxima with $\{\phi,\psi\}_C$ = 7°,4°; 101°,61° and 94°,−50°. The conformational distribution function of the D−E fragment exhibits problems similar to those of the C−D fragment but with only a single maximum centered at $\{\phi,\psi\}_D$ = 11°,11°. The $\{\phi,\psi\}_C$ = 7°,4° conformation violates the exo-anomeric effect,[66] and the doubly eclipsed conformation is therefore highly improbable. In fact, the analysis of the MD trajectory (Figures 3c and 4e,f) does not indicate this conformation. The population of this conformation is probably a result of the limited number of experimental parameters and their limited sensitivity to the conformational details. Thus, to improve the conformational description of the C−D fragment, we needed to increase the experimental data set.

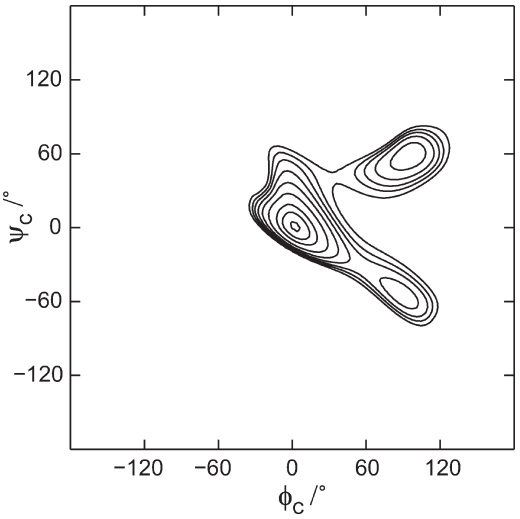

Figure 7. Population distribution of ϕ_C versus ψ_C for the β-(1 → 3) linkage between C and D in LNF-1 calculated from experimental J couplings and T-ROE parameters using eqs 7 and 9.

In addition to J couplings, T-ROE parameters, and dipolar couplings, another NMR parameter is also available for conformational analysis, namely, the nuclear spin relaxation.[83] This parameter has frequently been employed in investigations of biological molecules in general[84,85] and carbohydrates in particular.[86,87] The model proposed by Lipari and Szabo (LS)[88] is often used for the interpretation of experimental relaxation results. In this model, the molecular dynamics is separated into two contributions: the global molecular motion is described by a single correlation time, whereas the internal motion, related to conformational transitions, is characterized by the time correlation function (TCF), $C_I(t)$. This internal correlation function reflects the fast local dynamics in the molecule, but here, we focus on the geometrical information provided by the long-time limit of this TCF: $C_I(\infty) = S^2$, where S^2 is called the generalized order parameter. In fact, a nuclear spin relaxation investigation of LNF-1 was previously reported[41] in which carbon-13 relaxation times were measured. The interpretation of the experimental results, employing the LS model that provided S^2 values for several C−H vectors in the LNF-1 molecule, is compiled in Table 5. The S^2 parameter can also be expressed as[88]

$$S^2 = \iint P(\Omega_1)\,P_2(\cos\varphi_{12})\,P(\Omega_2)\,d\Omega_1\,d\Omega_2 \quad (10)$$

where Ω_1 and Ω_2 are conformations defined by ϕ and ψ and $P(\Omega_i)$ is the corresponding normalized probability distribution function. The second-order Legendre polynomial is denoted as $P_2(\cos\varphi_{12})$, where φ_{12} is the angle between the C−H vector in conformations Ω_1 and Ω_2. To calculate this angle, all conformations—and therefore the coordinates of the relevant atoms—must be expressed in a common frame. In practice, this frame is obtained by superimposing the atomic coordinates for all conformations of the relevant molecular fragment. The discussion here is limited to the molecular fragment consisting of residues C and D in LNF-1. A detailed description of the superimposing procedure can be found in ref 89; here, we summarize the basic steps in this approach: (i) The atomic coordinates for all

Table 5. Generalized Order Parameters (S^2) for the C−H Vectors in LNF-1 Derived from the Experimental Relaxation Data[41] and from eq 10

	S^2			
vector	axial model, expt[a]	three-state model[b]	two-state model[c]	modified two-state model[d]
C1C−H1C	0.72	0.46	0.60	0.77
C2C−H2C	0.72	0.46	0.61	0.77
C3C−H3C	0.72	0.46	0.62	0.76
C4C−H4C	0.72	0.44	0.60	0.80
C5C−H5C	0.72	0.43	0.60	0.78
C1D−H1D	0.60	0.43	0.45	0.70
C2D−H2D	0.60	0.43	0.44	0.70
C3D−H3D	0.60	0.43	0.40	0.67
C5D−H5D	0.60	0.44	0.46	0.71

[a] Error bounds for one standard deviation are 0.05. [b] $\{\phi,\psi\}_C$ = 7°,4°; 101°,61°; 94°,−50°. [c] $\{\phi,\psi\}_C$ = 101°,61°; 94°,−50°. [d] $\{\phi,\psi\}_C$ = 44°, 39°; 39°,−40°.

conformations are translated so that the center of mass of the fragment is located at the origin. (ii) The conformation corresponding to the largest moment of inertia, $I = {}^1/_3(I_{xx} + I_{yy} + I_{zz})$, is selected as the reference fragment. (iii) The atomic coordinates of all of the conformations are rotated into the reference coordinates. This step is carried out by defining three laboratory-fixed planes, namely, *XY*, *XZ*, and *YZ*, projecting the coordinates onto these planes, and then performing rotations (about the *Z*, *Y*, and *X* axes) of all of the conformations into the reference frame. The rotation in the *XY* plane is defined by the rotation matrix $R_Z(\beta)$, and the rotation angle β is defined as

$$\beta = \mathrm{Arg}\left[\sum_{k=1}^{N} m_k(X_k + \mathrm{i}Y_k)^*(X_k^{\mathrm{ref}} + \mathrm{i}Y_k^{\mathrm{ref}})\right] \qquad (11)$$

where Arg is the complex argument and the asterisk indicates the complex conjugate. The number of atoms in the fragment is *N*; m_k is the atomic mass, which is used for weighting; and the superscript ref indicates the atoms of the reference conformation. This step is repeated until the rotation angle is zero for all three planes. (iv) A new reference fragment is obtained as an average over all conformations by calculating the probability-weighted coordinates. In the averaging, a conformational distribution is assumed. Steps iii and iv are repeated until the reference fragment does not change.

We are now in a position to calculate S^2 for the C−H vectors in LNF-1 using the three-state distribution shown in Figure 7 and assuming $P(\Omega_1) = P(\Omega_2) = P(\Omega_3) = {}^1/_3$. Note that the angle φ_{12} in eq 10 reflects the relations between all three states in this distribution. The values of S^2 are clearly lower than those derived from the experiments (Table 5) for all vectors in the C and D sugar residues. This result is consistent with our expectations, as the state $\{\phi,\psi\}_C$ = 7°,4° is highly improbable. By removing this state, the agreement between the calculated and experimental S^2 values increases significantly. We can therefore assume that the state $\{\phi,\psi\}_C$ = 7°,4° is an artifact of the analysis. Finally, we note that the generalized order parameter is rather sensitive to the ψ values of the two remaining states. By changing the ψ values from 60° and −50° to 39° and −40°, respectively, a significant improvement was obtained (Table 5). In fact, the latter ψ torsion-angle averages correspond to those derived from the MD simulation.

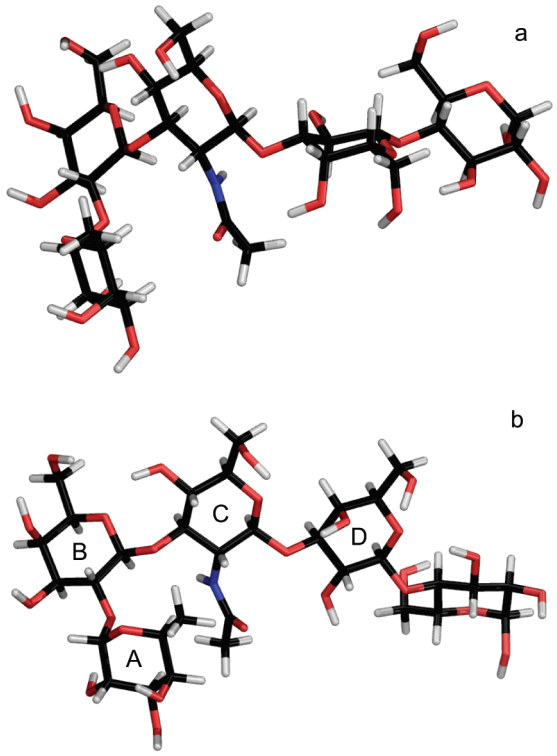

Figure 8. Molecular models of LNF-1 from the MD simulations as a result of two significantly populated conformational states at the (1→3) linkage between residues C and D, with (a) $\langle\psi_C^+\rangle$ = 39° and (b) $\langle\psi_C^-\rangle$ = −40°.

CONCLUSIONS

Using NMR spectroscopy techniques, the conformational transitions of LNF-1 have been studied in isotropic solution and in an oriented medium. The latter facilitates the acquisition of additional data, both hetero- and homonuclear RDCs, which are helpful in describing the complex conformational equilibria of the oligosaccharide but which require quite a few observables for a conclusive interpretation. From the conformational distribution of states observed in the MD simulation, NMR observables or related properties were calculated and found to be in good to excellent agreement with the measured NMR data. The terminal trisaccharide part having the fucosyl group in LNF-1 exhibits a well-defined structure in which only occasional transitions to other conformational regions occur. At the reducing end, which has a lactosyl group, frequent transitions take place at the ψ_C torsion angle, leading to two conformational states of approximately equal populations (Figure 8) with $\tau_N < \tau_M$; that is, the internal dynamics occur on a shorter time scale than the overall rotation of the molecule. The additional use of generalized order parameters from nuclear spin relaxation experiments in the analysis of oligosaccharide conformational dynamics where nuclear Overhauser effects, trans-glycosidic coupling constants, and residual dipolar couplings are combined to generate probability distributions for the torsion angles at glycosidic linkages might be worth including in future analysis protocols, as indicated by the present results, in which the extent of flexibility at a glycosidic linkage could be estimated. From a biological

dx.doi.org/10.1021/jp2017105 |J. Phys. Chem. B 2011, 115, 7109–7121

point of view, the terminal α-(1 → 2)-linked fucosyl residue of the oligosaccharide is part of a well-defined structure, and the resulting epitope might be a key factor in protection against infant diarrhea. The question of whether the lactosyl group is just a suitable scaffold onto which the trisaccharide epitope is attached or whether the flexibility is an important part in the biological response of human milk oligosaccharides remains to be elucidated.

AUTHOR INFORMATION

Corresponding Author
*E-mail: gw@organ.su.se.

ACKNOWLEDGMENT

This work was supported by grants from the Swedish Research Council, the Knut and Alice Wallenberg Foundation, and the Swedish National Infrastructure for Computing.

REFERENCES

(1) Meyer, B.; Peters, T. *Angew. Chem., Int. Ed.* **2003**, *42*, 864–890.
(2) Driscoll, P. C.; Gronenborn, A. M.; Beress, L.; Clore, G. M. *Biochemistry* **1989**, *28*, 2188–2198.
(3) Stolarski, R.; Egan, W.; James, T. L. *Biochemistry* **1992**, *31*, 7027–7042.
(4) Kogelberg, H.; Frenkiel, T. A.; Homans, S. W.; Lubieneau, A. *Biochemistry* **1995**, *35*, 1954–1964.
(5) Tjandra, N.; Bax, A. *J. Magn. Reson.* **1997**, *124*, 512–515.
(6) Prestegard, J. H.; Al-Hashimi, H. M.; Tolman, J. R. *Q. Rev. Biophys.* **2000**, *33*, 371–424.
(7) Lawson, K. D.; Flautt, T. J. *J. Am. Chem. Soc.* **1967**, *89*, 5489–5491.
(8) Sanders, C. R.; Schwonek *Biochemistry* **1992**, *31*, 8898–8905.
(9) van Dam, L.; Karlsson, G.; Edwards, K. *Langmuir* **2006**, *22*, 3280–3285.
(10) Cavagnero, S.; Dyson, H. J.; Wright, P. E. *J. Biomol. NMR* **1999**, *13*, 387–391.
(11) Gabriel, J.-C. P.; Camerel, F.; Lemaire, B. J.; Desvaux, H.; Davidson, P.; Batail, P. *Nature* **2001**, *413*, 504–508.
(12) Barrientos, L. G.; Dolan, C.; Gronenborn, A. M. *J. Biomol. NMR* **2000**, *16*, 329–337.
(13) Meier, S.; Blackledge, M.; Grzesiek, S. *J. Chem. Phys.* **2008**, *128*, 052204.
(14) Lakomek, N. A.; Carlomango, T.; Becker, S.; Griesinger, C.; Meiler, J. *J. Biomol. NMR* **2006**, *34*, 101–115.
(15) Bermel, W.; Tkach, E. N.; Sobol, A. G.; Golovanov, A. P. *J. Am. Chem. Soc.* **2009**, *131*, 8564–8570.
(16) Nodet, G.; Salmon, L.; Ozenne, V.; Meier, S.; Ringkjøbing Jensen, M.; Blackledge, M. *J. Am. Chem. Soc.* **2009**, *131*, 17908–17918.
(17) Zeng, J.; Boyles, J.; Tripathy, C.; Wang, L.; Yan, A.; Zhou, P.; Donald, B. R. *J. Biomol. NMR* **2009**, *45*, 265–281.
(18) Donald, B. R.; Martin, J. *Prog. Nucl. Magn. Reson. Spectrosc.* **2009**, *55*, 101–127.
(19) Miner, V. W.; Tyrell, P. M.; Prestegard, J. H. *J. Magn. Reson.* **1983**, *55*, 438–452.
(20) Prestegard, J. H.; Miner, V. W.; Tyrell, P. M. *Proc. Natl. Acad. Sci. U.S.A.* **1983**, *80*, 7192–7196.
(21) Tyrell, P. M.; Prestegard, J. H. *J. Am. Chem. Soc.* **1986**, *108*, 3990–3995.
(22) Ram, P.; Mazzola, L.; Prestegard, J. H. *J. Am. Chem. Soc.* **1989**, *111*, 3676–3682.
(23) Kummerlöwe, G.; Luy, B. *Annu. Rev. NMR Spectrosc.* **2009**, *68*, 193–230.
(24) Rundlöf, T.; Landersjö, C.; Lycknert, K.; Maliniak, A.; Widmalm, G. *Magn. Reson. Chem.* **1998**, *36*, 773–776.
(25) Kiddle, G. R.; Homans, S. W. *FEBS Lett.* **1998**, *436*, 128–130.
(26) Bolon, P. J.; Prestegard, J. H. *J. Am. Chem. Soc.* **1998**, *120*, 9366–9367.
(27) Thaning, J.; Stevensson, B.; Östervall, J.; Naidoo, K. J.; Widmalm, G.; Maliniak, A. *J. Phys. Chem. B* **2008**, *112*, 834–836.
(28) Silpo, A.; Zhang, Z.; Javier Cañada, F.; Molinaro, A.; Linhardt, R. J. *ChemBioChem* **2008**, *9*, 240–252.
(29) Jin, L.; Hricovíni, M.; Deakin, J. A.; Lyon, M.; Uhrín, D. *Glycobiology* **2009**, *19*, 1185–1196.
(30) Gargiulo, V.; Morando, M. A.; Silipo, A.; Nurisso, M. A.; Pérez, S.; Imberty, A.; Javier Cañada, F.; Parrilli, M.; Jiménez-Barbero, J.; De Castro, C. *Glycobiology* **2010**, *20*, 1208–1216.
(31) Ganguly, S.; Xia, J.; Margulis, C.; Stanwyck, L.; Bush, C. A. *Biopolymers* **2011**, *95*, 39–50.
(32) Kuhn, R. *Bull. Soc. Chim. Biol.* **1958**, *40*, 297–314.
(33) Kunz, C.; Rudloff, S.; Baier, W.; Klein, N.; Strobel, S. *Annu. Rev. Nutr.* **2000**, *20*, 699–722.
(34) Newburg, D. S.; Ruiz-Palacios, G. M.; Altaye, M.; Chaturvedi, P.; Meinzen-Derr, J.; de Luordes Guerrero, M.; Morrow, A. L. *Glycobiology* **2004**, *14*, 253–263.
(35) Hakkarainen, J.; Toivanen, M.; Leinonen, A.; Frängsmyr, L.; Strömberg, N.; Lapinjoki, S.; Nassif, X.; Tikkanen-Kaukanen, C. *J. Nutr.* **2005**, *135*, 2445–2448.
(36) Perret, S.; Sabin, C.; Dumon, C.; Pokorná, M.; Gautier, C.; Galanina, O.; Ilia, S.; Bovin, N.; Nicaise, M.; Desmadril, M.; Gilboa-Garber, N.; Wimmerová, M.; Mitchell, E. P.; Imberty, A. *Biochem. J.* **2005**, *389*, 325–332.
(37) Hermansson, K.; Jansson, P.-E.; Kenne, L.; Widmalm, G.; Lindh, F. *Carbohydr. Res.* **1992**, *235*, 69–81.
(38) Uhrín, D. *J. Magn. Reson.* **2002**, *159*, 145–150.
(39) Rao, B. N. N.; Dua, V. K.; Bush, C. A. *Biopolymers* **1985**, *24*, 2207–2229.
(40) Cagas, P.; Kaluarachchi, K.; Bush, C. A. *J. Am. Chem. Soc.* **1991**, *113*, 6815–6822.
(41) Rundlöf, T.; Venable, R. M.; Pastor, R. W.; Kowalewski, J.; Widmalm, G. *J. Am. Chem. Soc.* **1999**, *121*, 11847–11854.
(42) Manuel-Pastor, M.; Bush, C. A. *Biochemistry* **2000**, *39*, 4674–4683.
(43) Almond, A.; Petersen, B. O.; Duus, J. Ø. *Biochemistry* **2004**, *43*, 5853–5863.
(44) Xia, J.; Daly, R. P.; Chuang, F.-C.; Parker, L.; Jensen, J. H.; Margulis, C. J. *J. Chem. Theory Comput.* **2007**, *3*, 1629–1643.
(45) Xia, J.; Margulis, C. *J. Biomol. NMR* **2008**, *42*, 241–256.
(46) Kjellberg, A.; Widmalm, G. *Biopolymers* **1999**, *50*, 391–399.
(47) Hwang, T.-L.; Shaka, A. J. *J. Magn. Reson. B* **1993**, *102*, 155–165.
(48) Kupče, Ē.; Boyd, J.; Campbell, I. D. *J. Magn. Reson. B* **1995**, *106*, 300–303.
(49) Nishida, T.; Widmalm, G.; Sándor, P. *Magn. Reson. Chem.* **1996**, *34*, 377–382.
(50) Meissner, A.; Sørensen, O. W. *Magn. Reson. Chem.* **2001**, *39*, 49–52.
(51) Tjandra, N.; Bax, A. *J. Magn. Reson.* **1997**, *124*, 512–515.
(52) Delaglio, F.; Grzesiek, S.; Vuister, G. W.; Zhu, G.; Pfeifer, J.; Bax, A. *J. Biomol. NMR* **1995**, *6*, 277–293.
(53) Delaglio, F.; Wu, Z.; Bax, A. *J. Magn. Reson.* **2001**, *149*, 276–281.
(54) Otting, G.; Rückert, M.; Levitt, M. H.; Moshref, A. *J. Biomol. NMR* **2000**, *16*, 343–346.
(55) Brooks, B. R.; Bruccoleri, R. E.; Olafson, B. D.; States, D. J.; Swaminathan, S.; Karplus, M. *J. Comput. Chem.* **1983**, *4*, 187–217.
(56) MacKerell, A. D., Jr.; Bashford, D.; Bellott, M.; Dunbrack, R. L., Jr.; Evanseck, J. D.; Field, M. J.; Fischer, S.; Gao, J.; Guo, H.; Ha, S.; Joseph-McCarthy, D.; Kushnir, L.; Kuczera, K.; Lau, F. T. K.; Mattos, C.; Michnick, S.; Ngo, T.; Nguyen, T. D.; Prodhom, B.; Reiher, W. E., III; Roux, B.; Schlenkrich, M.; Smith, J. C.; Stote, R.; Straub, J.; Watanabe, M.; Wiórkiewicz-Kuczera, J.; Yin, D.; Karplus, M. *J. Phys. Chem. B* **1998**, *102*, 3586–3616.
(57) Eklund, R.; Widmalm, G. *Carbohydr. Res.* **2003**, *338*, 393–398.
(58) Neria, E.; Fischer, S.; Karplus, M. *J. Chem. Phys.* **1996**, *105*, 1902–1921.

(59) Hockney, R. W. *Methods Comput. Phys.* **1970**, *9*, 136–211.
(60) Ryckaert, J. P.; Ciccotti, G.; Berendsen, H. J. C. *J. Comput. Phys.* **1977**, *23*, 327–341.
(61) Berendsen, H. J. C.; Postma, J. P. M.; van Gunsteren, W. F.; DiNola, A.; Haak, J. R. *J. Chem. Phys.* **1984**, *81*, 3684–3690.
(62) Steinbach, P. J.; Brooks, B. R. *J. Comput. Chem.* **1994**, *15*, 667–683.
(63) Fehér, K.; Berger, S. *J. Magn. Reson.* **2004**, *170*, 191–198.
(64) Prestegard, J. H.; Bougault, C. M.; Kishore, A. I. *Chem. Rev.* **2004**, *104*, 3519–3540.
(65) Tolman, J. R.; Al-Hashimi, H. M.; Kay, L. E.; Prestegard, J. H. *J. Am. Chem. Soc.* **2001**, *123*, 1416–1424.
(66) Lemieux, R. U.; Pavia, A. A.; Martin, J. C.; Watanabe, K. A. *Can. J. Chem.* **1969**, *47*, 4427–4439.
(67) Loncharich, R. J.; Brooks, B. R.; Pastor, R. W. *Biopolymers* **1992**, *32*, 523–535.
(68) Pastor, R. W. In *The Molecular Dynamics of Liquid Crystals*; Luckhurst, G. R., Veracini, C. A., Eds.; Kluwer: Dordrecht, The Netherlands, 1994; pp 85−138.
(69) Zwanzig, R.; Ailawadi, N. K. *Phys. Rev.* **1969**, *182*, 280–283.
(70) Feller, S. E.; Pastor, R. W.; Rojnuckarin, A.; Bogusz, S.; Brooks, B. R. *J. Phys. Chem.* **1996**, *100*, 17011–17020.
(71) Venable, R. M.; Hatcher, E.; Guvench, O.; MacKerell, A. D., Jr.; Pastor, R. W. *J. Phys. Chem. B* **2010**, *114*, 12501–12507.
(72) Mills, R.; Harris, K. R. *Chem. Soc. Rev.* **1976**, *5*, 215–231.
(73) Jas, G. S.; Eaton, W. A.; Hofrichter, J. *J. Phys. Chem. B* **2001**, *105*, 261–272.
(74) Zerbetto, M.; Polimeno, A.; Kotsyubynskyy, D.; Ghalebani, L.; Kowalewski, J.; Meirovitch, E.; Olsson, U.; Widmalm, G. *J. Chem. Phys.* **2009**, *131*, 234501.
(75) Zhang, W.; Zhao, H.; Carmichael, I.; Serianni, A. S. *Carbohydr. Res.* **2009**, *344*, 1582–1587.
(76) Coxon, B. *Adv. Carbohydr. Chem. Biochem.* **2009**, *62*, 17–82.
(77) Cloran, F.; Carmichael, I.; Serianni, A. S. *J. Am. Chem. Soc.* **1999**, *121*, 9843–9851.
(78) Tvaroska, I.; Taravel, F. R. *J. Biomol. NMR* **1992**, *2*, 421–430.
(79) Widmalm, G.; Venable, R. M. *Biopolymers* **1994**, *34*, 1079–1088.
(80) Catalano, D.; Di Bari, L.; Veracini, C. A.; Shilstone, G. N.; Zannoni, C. *J. Chem. Phys.* **1991**, *94*, 3928–3935.
(81) Berardi, R.; Spinozzi, F.; Zannoni, C. A *J. Chem. Phys.* **1998**, *109*, 3742–3759.
(82) *MATLAB*; The MathWorks: Natick, MA, 1999.
(83) Kowalewski, J.; Mäler, L. *Nuclear Spin Relaxation in Liquids: Theory, Experiments, and Applications*; CRC Press: Boca Raton, FL, 2006.
(84) Bracken, C. *J. Mol. Graph. Modell.* **2001**, *19*, 3–12.
(85) Chen, K.; Tjandra, N. *J. Magn. Reson.* **2009**, *197*, 71–76.
(86) Söderman, P.; Widmalm, G. *Magn. Reson. Chem.* **1999**, *37*, 586–590.
(87) Dais, P.; Tylianakis, E.; Kanetakis, J.; Taravel, F. R. *Biomacromolecules* **2005**, *6*, 1397–1404.
(88) Lipari, G.; Szabo, A. *J. Am. Chem. Soc.* **1982**, *104*, 4546–4559.
(89) Gerber, P. R.; Müller, K. *Acta Crystallogr. A* **1987**, *43*, 426–428.